https://doi.org/10.1016/j.jechem.2021.04.020

This is the Pre-Published Version.

Achieving Exceptional Activity and Durability Toward Oxygen Reduction Based on a Cobalt-Free Perovskite for Solid Oxide Fuel Cells

Feifei Dong,[†] Zhenghui Gao,[†] Bingkai Zhang,[†] Lu Li,[†] Ziqi Kong,[†] Zilin Ma,[†] Bowen Yao,[†] Meng Ni,[‡] and Zhan Lin*[,†]

[†]Guangzhou Key Laboratory of Clean Transportation Energy Chemistry, School of Chemical Engineering and Light Industry, Guangdong University of Technology, Guangzhou Higher Education Mega Center, Guangzhou 510006, P. R. China

[‡]Building Energy Research Group, Department of Building and Real Estate, The Hong Kong Polytechnic University, Hung Hom, Kowloon, Hong Kong 999077, P. R. China

KEYWORDS: solid oxide fuel cells, cathodes, perovskites, oxygen reduction reaction, cobalt-free

ABSTRACT: In response to the shortcomings of cobalt-rich cathodes, iron-based perovskite oxides appear as promising alternatives for solid oxide fuel cells (SOFCs). However, their inferior electrochemical performance at reduced temperatures (< 700 °C) becomes a major bottleneck for future progress. Here, a novel cobalt-free perovskite $Ba_{0.75}Sr_{0.25}Fe_{0.875}Ga_{0.125}O_{3-\delta}$ (BSFG) is developed as an efficient oxygen reduction electrode for SOFCs, featuring cubic-symmetry structure, large oxygen vacancy concentration and fast oxygen transport. Benefiting from these merits, cells incorporated with BSFG achieve exceptionally high electrochemical performance, as evidenced by a low polarization area-specific resistance of 0.074 Ω cm^2 and a high peak power density of 1145 mW cm^{-2} at 600 °C. Meanwhile, a robust short-term performance stability of BSFG cathode can be ascribed to the stable crystalline structure and favorable thermal expansion behavior. First-principles computations are also conducted to understanding the superior activity and durability toward oxygen reduction reaction. These pave the way for rationally developing highly active and robust cobalt-free perovskite-type cathode materials for reduced-temperature SOFCs.

The global energy demand has aroused considerable interest in solid oxide fuel cells (SOFCs), enabling direct electrochemical generation of electrical energy from chemical energy in fuels with high efficiency, low emission, as well as excellent fuel flexibility.[1,2] To tackle the cost and degradation issues due to high temperature operation of conventional SOFCs, research efforts have concentrated on lowering the operating temperature toward an intermediate-to-low temperature range (500-700 °C).[3] However, due to the sluggish kinetics of the oxygen reduction reaction (ORR), the increased cathode polarization resistance at reduced temperatures is a primary contributor to the overall resistance of SOFCs, resulting in the device degradation in performance and efficiency.[4] Numerous efforts have been strived to explore alternative cathode materials with high electrocatalytic activity and durability for ORR to make SOFCs economically competitive and commercially viable.[5-7]

Over the past decades, mixed ionic-electronic conducting perovskite oxides have been considered one of the landmarks in cathode development. Such mixed conductivity can open up the reaction active sites from the three-phase boundary to the entire surface of cathode materials.[8] Among the exploited perovskite family, abundant cobalt-containing perovskite oxides exhibit attractive electrochemical activity at intermediate temperatures as cathode materials for SOFCs. Examples include $Sm_{0.5}Sr_{0.5}CoO_{3-\delta}$, $Ba_{0.5}Sr_{0.5}Co_{0.8}Fe_{0.2}O_{3-\delta}$ (BSCF), $La_{0.6}Sr_{0.4}Co_{0.2}Fe_{0.8}O_{3-\delta}$ (LSCF), $Sr_{0.95}Co_{0.8}Nb_{0.1}Ta_{0.1}O_{3-\delta}$, $BaCo_{0.4}Fe_{0.4}Zr_{0.1}Y_{0.1}O_{3-\delta}$ (BCFZY), $PrBa_{0.5}Sr_{0.5}Co_{1.5}Fe_{0.5}O_{5+\delta}$, $Eu_2SrCo_{1.5}Fe_{0.5}O_7$.[9-15] Nevertheless, the wide-spread adoption of these materials is generally restrained by several drawbacks, such as high price of cobalt, poor structural stability, abnormally high thermal expansivity, and inadequate compatibility with the electrolyte.[16]

Alternatively, as a cobalt-free mixed conducting perovskite, $BaFeO_{3-\delta}$ (BF) stands out as a promising parent oxide for cathode materials owing to its feasible electrocatalytic activity for ORR.[17] This could be validated by the low divalent oxidation state and large ionic radius of Ba ions, as well as the variable oxidation states and high chemical and thermal stability of Fe ions. However, pristine BF exists in diverse phase structures depending on the oxygen deficiency, which is sensitive to synthesis conditions.[18,19] Doping strategy is commonly adopted to stabilize the oxygen vacancy-disordered cubic-symmetry lattice, which can maximize the oxygen ion conduction through three-dimensional transport channels, thus promoting the ORR. In this regard, various cations have been substituted into BF crystal, such as La, Ce, Sm, Gd, Y in the A-site, or Nb, Y, Ce, Zr, Ca, Cu in the B-site for better beneficial properties.[20-26] Nonetheless, the insufficient electrochemical performance of these materials is still inferior to that of the state-of-art cobalt-based counterparts (e.g., BSCF) at reduced temperatures. With regard to the top-performing perovskite materials, it is generally favorable to contain alkaline earth elements on the A-site and a mixture of late transition metals (e.g., Co and Fe) and less redox-active elements on the B-site.[27] Also, co-doping in A or B site of perovskite cathodes is evidenced to boost the physicochemical properties.[5,12,28] Inspired by that, there is a strong motivation to develop co-substituted BF-based perovskite-type oxygen catalysts with improved activity and stability. In addition, few

© 2021. This manuscript version is made available under the CC-BY-NC-ND 4.0 license https://creativecommons.org/licenses/by-nc-nd/4.0/

studies report the possible mechanism of co-substitution with appropriate dopants to stabilize the cubic phase of BF parent oxide.

Herein, to acquire desirable electrochemical performance at reduced temperatures, we present a new cobalt-free perovskite $Ba_{0.75}Sr_{0.25}Fe_{0.875}Ga_{0.125}O_{3-\delta}$ (BSFG) as a prominent cathode material for SOFCs. This Sr^{2+} and Ga^{3+} co-doped BF perovskite system is preferred on the basis of the following factors: well-preserved cubic crystalline structure, large oxygen vacancy content, rapid oxygen surface exchange and bulk diffusion, favorable thermal expansion coefficient (TEC). Accordingly, when incorporating into samarium-doped ceria (SDC) electrolyte-based symmetrical and single cells, BSFG cathode exhibits exceptional electrochemical performance, manifested by a low polarization area-specific resistance (ASR) of 0.074 Ω cm^2 and a high peak power density (PPD) of 1145 mW cm^{-2} without noticeable performance degradation for 50 h at 600 °C. We also unravel the underlying mechanisms of the remarkable activity and durability of BSFG for ORR, providing a strategy vital to rationally designing highly active and durable perovskite-type cathode materials for SOFCs.

The crystallization phase of BSFG was first identified by X-ray diffraction (XRD). As described previously by our group, the parent oxide BF adopted a complicated crystal structure, consisting of a cubic phase ($BaFeO_3$, space group: *Pm*-3*m*), an orthorhombic phase ($BaFe_2O_4$, space group: *Cmc*21), and a monoclinic phase ($Ba_2Fe_2O_5$, space group *P*121/*c*1).[22] Satisfactorily, co-substitution with Sr and Ga cations facilitated the formation of a single-phase perovskite structure. Rietveld refinement of XRD data in Figure 1a revealed that the BSFG crystallizes in a cubic-symmetry perovskite structure with a lattice parameter of a = 4.0300(8) Å and a space group of *Pm*-3*m* (for full details of the refinement see Table S1). A reliable refinement fit was achieved based on low reliability factors of R_p = 7.07%, R_{wp} = 9.56%, and χ^2 = 0.913. To further confirm the crystal structure of BSFG, high-resolution transmission electron microscopy (HR-TEM) was also implemented (Figure 1b). As seen in the magnified image in Figure 1c, clear lattice fringes with a d-spacing value of approximately 2.79(7) Å were observed, corresponding to the (110) diffraction plane in the cubic-symmetry perovskite phase. Furthermore, this cubic structure was clearly evidenced by the emergence of lattice spots in the fast Fourier transform (FFT) pattern oriented on [1$\bar{1}$0] zone axis (Figure 1c, inset). This result is in good accordance with that calculated based on the XRD data.

Considering the great importance of structural stability for cathode materials under operating conditions, we examined the phase stability of BSFG by annealing the material in static air at 600 °C for 100 h and subsequent refined XRD (Figure S1). BSFG preserves its original cubic phase structure, and analogous crystal lattice parameters are obtained resulting from Rietveld refinement, demonstrating the prominent structural stability of BSFG perovskite oxide.

As an essential factor for durable operation of cathode materials at high temperatures, favorable TEC can restrain the occurrence of cracks or delamination at the cathode-electrolyte interface. As reflected by data-fitting of dL/L_0 as a function of temperature from 400-800 °C in Figure S2, the TEC value of BSFG is approximately 17.8×10^{-6} K^{-1}, which is lower than that of prevailing cobalt-enriched perovskites (e.g., 23.6×10^{-6} K^{-1} for BSCF) and even reported iron-based counterparts (e.g.,

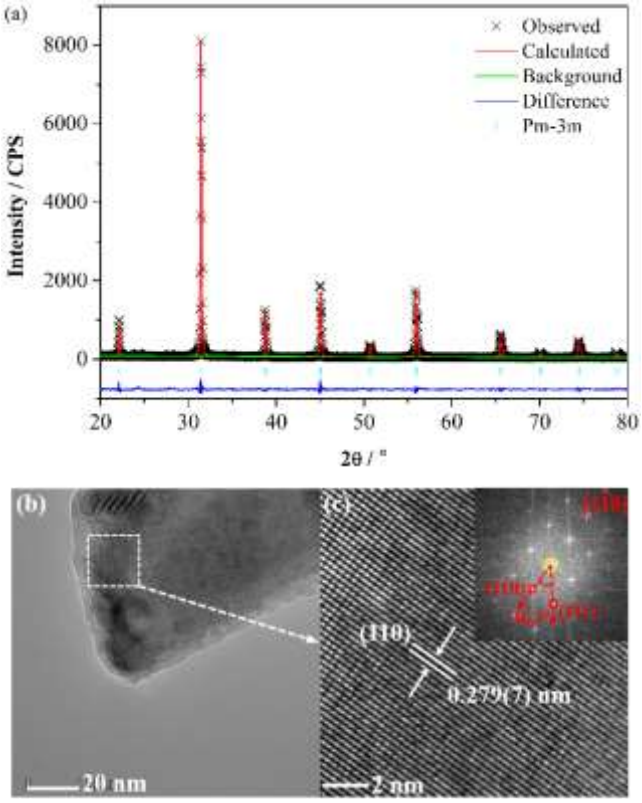

Figure 1. Crystal structure of BSFG. a) refined XRD patterns of BSFG powder. b) HR-TEM image of BSFG. c) The magnified view and the corresponding FFT pattern (inset).

21.3×10^{-6} K^{-1} for $BaFe_{0.75}Ni_{0.25}O_{3-\delta}$).[13,29] This renders it superior thermal stability and compatibility with the electrolyte.

In accordance with the charge-transfer reaction of $O_{ads} + 2e^- + V_o^{\cdot\cdot} \rightleftharpoons O_o^x$ in cathode, the oxygen vacancy and electron concentrations and their diffusivity are identified as a significant contributor to the charge-transfer process. The oxygen vacancies at room temperature and elevated temperatures were explored by iodometric titration and thermogravimetric analysis (TGA), respectively. At room temperature, the average valence state of iron cation in BSFG is determined to be 3.21, and the oxygen non-stoichiometry is estimated to be 0.41. Owing to the isovalent or lower-valent nature of the substitutions (Sr^{2+} and Ga^{3+}) in comparison to the corresponding cations (Ba^{2+} and Fe^{3+}/Fe^{4+}), the oxygen concentration is higher than those of other doped BF parent materials with higher-valent cations, such as La^{3+}, Zr^{4+}, Nb^{5+}.[23,24,30] As can be seen from the TGA profile (Figure S3), a distinct weight loss of the BSFG sample was initiated at ~400 °C and continued up to 800 °C. This process can be attributed to oxygen release from the crystal lattice with the concomitant generation of oxygen vacancies, followed by the thermal reduction of iron cation due to the electroneutrality requirement.

Figure 2 shows the declined average valence of iron and resultantly increased oxygen vacancies as the temperature rises. The oxygen non-stoichiometry value of BSFG is approximately 0.49 ~ 0.57 over the temperature range for fuel cell operation (500-700 °C). Since vacancy sites can facilitate diffusion via oxygen hopping, such a high oxygen vacancy concentration is in favor of the fast migration of oxygen ions and thus the

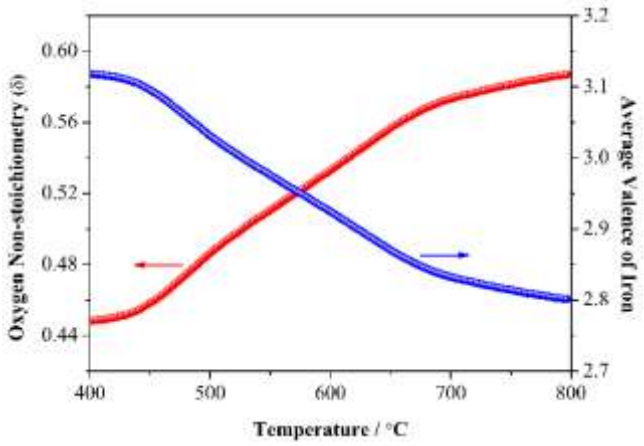

Figure 2. Thermogravimetric data of BSFG presenting a variation of oxygen non-stoichiometry and average valence state of iron ions with temperature.

improved ORR activity. Accordingly, the oxygen mobility is further reflected by the oxygen bulk diffusion coefficient (D_{chem}) and surface exchange coefficient (k_{chem}) via an electrical conductivity relaxation (ECR) method. As illustrated from the typical ECR response at 600 °C when abruptly switching the oxygen partial pressure (Figure S4), BSFG oxide takes a short relaxation time to reach a new equilibrium state, suggesting a rapid response to the change of ambient oxygen environment. Both D_{chem} and k_{chem} can be obtained by means of the fitting of ECR measurement. BSFG achieves a remarkable oxygen transference, e.g., $D_{chem} = 2.31\times10^{-4}$ cm^2 s^{-1} and $k_{chem} = 2.19\times10^{-3}$ cm s^{-1} at 600 °C, which is much higher than those of recently reported iron-based perovskite oxides[31,32] and even competitive with those of top-performing cobalt-based perovskite cathodes.[33,34] It follows that the stable cubic lattice structure and high oxygen deficiency are beneficial for distinguished oxygen bulk diffusion and surface exchange properties, which in turn boosts ORR capability. Moreover, as shown in Figure S5, the electrical conductivity of BSFG decreases gradually with an increase in temperature (400-800 °C), pointing to a n-type metallic-conductor-like behavior. This could be rationalized by noting that the created more oxygen vacancies originating from the reduction of iron cation at high temperatures, as evidenced by the TGA in Figure S3, would block the migration of localized electrons via the Fe-O-Fe double exchange mechanism. BSFG oxide possesses acceptable electrical conductivities at the working temperature range of fuel cell, which is comparable to those of other doped BF materials.[35,36]

To assess the ORR activity of BSFG cathode, we measured the electrochemical impedance spectroscopy (EIS) of a symmetrical cell of BSFG fabricated on SDC electrolyte under open circuit conditions. Figure 3a depicts the Nyquist-type plots of EIS tested from 500 to 700 °C. For clarity of comparison, each impedance spectrum was ohmic-resistance-subtracted. The area-specific resistance (ASR) value can be extracted from the difference of intersections between the impedance arc and the real axis, representing the ORR activity of cathodes, and the data are illustrated in an Arrhenius plot in Figure 3b. The BSFG electrode delivers attractive ORR catalytic activity, with extremely low ASR values of 0.016, 0.074 and 0.61 Ω cm^2 at 700, 600 and 500 °C, respectively. The electroactivity of BSFG cathode substantially outperforms that of some advanced cobalt-free cathodes, including $Bi_2Sr_2Nb_2MnO_{12-\delta}$ (BSNM), $SrFeO_{2.95-\delta}F_{0.05}$ (SFF), $Bi_{0.5}Sr_{0.5}Fe_{0.90}Sb_{0.10}O_{3-\delta}$ (BSFS),

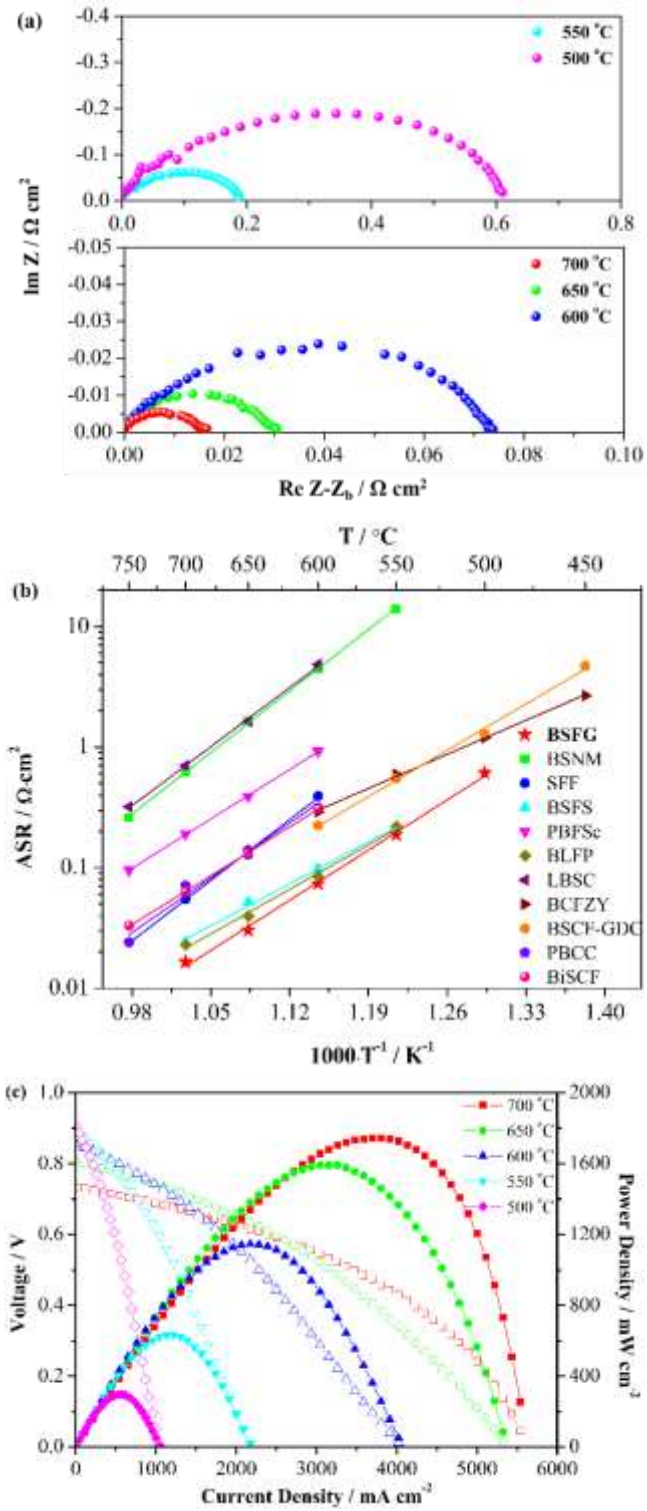

Figure 3. Electrochemical performance of the BSFG cathode. a) Nyquist plots of the BSFG cathode in a symmetrical cell configuration measured at 500-700 °C. b) Performance comparison of the ASR values of the BSFG cathode against other reported high-performance cobalt-free and cobalt-based cathodes. c) *I-V* and *I-P* curves of the anode-supported single cell with the BSFG cathode operating at 500-700 °C.

$PrBa(Fe_{0.8}Sc_{0.2})_2O_{5+\delta}$ (PBFSc), $Ba_{0.95}La_{0.05}Fe_{0.95}P_{0.05}O_{3-\delta}$ (BLFP), $La_{1.7}Bi_{0.2}Sr_{0.1}CuO_{4-\delta}$ (LBSC) (e.g., 0.393 Ω cm^2 for

SFF and ~4.5 Ω cm^2 for BSNM at 600 °C),[37-42] and is even superior or

Table 1. Performance comparison of PPD of the single cell with highly active iron-based and cobalt-based perovskite cathode materials measured at 600 °C.

Anode	Electrolyte	Cathode	PPD (mW cm^{-2})	Ref.
Ni-BZCYYb	GDC	LSCF fiber	620	46
Ni-SDC	SDC	SLFNT	1020	47
Ni-YSZ	YSZ-SDC	BFS	395	48
Ni-SDC	SDC	SFC	450	49
Ni-YSZ	YSZ-GDC	STFC	~550	50
Ni-SDC	SDC	SCFN	977	51
Ni-SDC	SDC	BSCF	1010	10
Ni-SDC	SDC	BCFY	967	52
Ni-SDC	SSZ	SBSC	1020	53
Ni-Fe	SDC-LSGM	SSC-SDC	1075	54
Ni-SDC	**SDC**	**BSFG**	**1145**	**This work**

LSCF: $La_{0.6}Sr_{0.4}Co_{0.2}Fe_{0.8}O_{3-\delta}$, SLFNT: $Sr_{0.95}Li_{0.05}Fe_{0.8}Nb_{0.1}Ta_{0.1}O_{3-\delta}$, BFS: $BaFe_{0.95}Sn_{0.05}O_{3-\delta}$, SFC: $Sr_3Fe_{1.8}Co_{0.2}O_{7-\delta}$, STFC: $SrTi_{0.3}Fe_{0.63}Co_{0.07}O_{3-\delta}$, SCFN: $Sr_{0.9}Ce_{0.1}Fe_{0.8}Ni_{0.2}O_{3-\delta}$, BSCF: $Ba_{0.5}Sr_{0.5}Co_{0.8}Fe_{0.2}O_{3-\delta}$, BCFY: $BaCo_{0.7}Fe_{0.22}Y_{0.08}O_{3-\delta}$, SBSC: $SmBa_{0.5}Sr_{0.5}Co_2O_{5+\delta}$, SSC: $Sm_{0.5}Sr_{0.5}CoO_{3-\delta}$

comparable to that of the widely representative cobalt-based cathodes, including BCFZY, BSCF-$Gd_{0.1}Ce_{0.9}O_{1.95}$ (BSCF-GDC), $PrBa_{0.8}Ca_{0.2}Co_2O_{5+\delta}$ (PBCC), $Bi_{0.15}Sr_{0.85}Co_{0.8}Fe_{0.2}O_{3-\delta}$ (BiSCF) (e.g., ~0.315 Ω cm^2 for PBCC and 0.31 Ω cm^2 for BiSCF),[13,43-45] with the detailed comparison of the temperature-dependent ASR shown in Figure 3b. This result is in accordance with the aforementioned analysis of structure and oxygen kinetics. Additionally, derived from the Arrhenius relation, a low activation energy (1.13 eV) of BSFG is observed, enabling its practical availability as an oxygen reduction electrode at low temperatures.

To further evaluate the suitability of BSFG cathode material in a practical fuel cell, we constructed an anode-supported cell with the configuration of Ni-SDC (anode) / SDC (electrolyte) / BSFG with the cross-sectional view shown in Figure S6. Figure 3c provides representative *I-V* and *I-P* curves of a single cell, collected with humidified H_2 and ambient air supplied to the anode and cathode, respectively. The cell yields significantly high PPDs of 1744 and 1145 mW cm^{-2} at 700 and 600 °C, respectively, which considerably surpass many iron-based perovskite cathode materials[46-51] and are comparable to the state-of-the-art benchmark cobalt-enriched perovskite cathode materials[10,52-54] as listed in Table 1, substantiating the outstanding electrocatalytic activity of BSFG under practical operating conditions. Taking into consideration the straightforward and cost-effective fabrication processes involved in this work, further advancement of output power density is achievable by employing well-tuned electrolytes (e.g., thinner-film by atomic layer deposition, functionally bi-layered electrolytes) and anodes (e.g., 3D architectural framework, integrated anode functional layer).

Furthermore, a short-term test was performed on the BSFG-derived single cell in a galvanostatic mode (1000 mA cm^{-2}) to verify the durability. As shown in Figure S7, the cell delivers a stable output voltage without noticeable performance

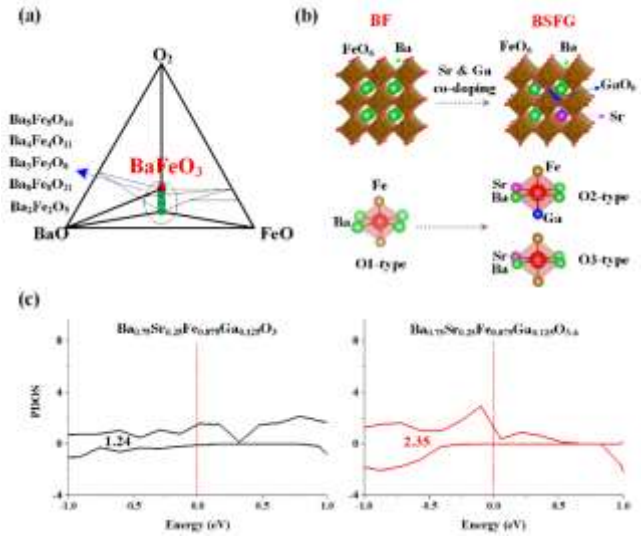

Figure 4. a) Ternary phase diagram of Ba-Fe-O system. b) Local structural units around oxygen in BF and BSFG. c) DOS near the Fermi level in δ = 0.13.

degradation at 600 °C for the test period of ~3000 min. After testing, it can be found that the BSFG electrode maintained porous structure with fine particles and firmly adhered to the electrolyte without delamination from the cross-sectional view (Figure S8), indicating robust structural characteristic and good thermal compatibility of BSFG with electrolyte. Thus, the favorably durable electrochemical performance of the BSFG cathode can arise from the stable perovskite lattice and compatible thermal expansion behavior, as referred to earlier. All above results make BSFG highly promising an air electrode for reduced-temperature SOFCs.

To gain fundamental insight into the structural stability and ORR activity of BSFG, we performed first-principles calculations to reveal the underlying mechanism in BSFG. The phase diagram of Ba-Fe-O system was simulated at 0 K as shown in Figure 4a. Ba_5FeO_{14}, $Ba_4Fe_4O_{11}$, $Ba_3Fe_3O_8$, $Ba_8Fe_8O_{21}$, $Ba_2Fe_2O_5$, and $BaFeO_3$ appear as stable phases that make up a convex hull, suggesting that the phase transformation among them is in accompany with oxygen release. This calculation results indicate that stable single-phase BF cannot exist in the Ba-Fe-O system. From the perspective of practical applications, the oxygen release is the most important factor to determine the thermal stability of Ba-Fe-O system. Therefore, for structural stability and ORR activity, the energy level required depends on the oxygen species in Ba-Fe-O crystal structure and their chemical bonding environment. Specifically, the local structural units in the Ba-Fe-O materials play a critical role in the redox process and participation of oxygen in them. In BF material, we find one type of structural unit around oxygen (or one local bonding environment around oxygen), that is, O1-type. After doping, there are two types of structural unit around oxygen (O2-type and O3-type) in BSFG as shown in Figure 4b. To show the difference for them, the oxygen vacancy formation energy was calculated as listed in Table 2. The results suggest that O2-type in BSFG is more stable than O1-type in BF and O3-type in BSFG. In other words, oxygen vacancy would likely occur in O3-type sites instead of O2-type sites in BSFG. BSFG thus would retain more O2-type oxygen,

contributing to the structural stability. This finding is valuable for BSFG since BF parent oxide has poor structural stability. In contrast, O3-type

Table 2. Oxygen vacancy formation energy of different types of structural unit around oxygen in BF and BSFG.

Oxygen vacancy concentration (δ)	O1-type	O2-type	O3-type
0.04	-0.67	-0.55	-0.91
0.08	-0.31	-0.28	-0.50
0.13	-0.07	0.30	0.06
0.17	0.14	0.76	0.40

oxygen in BSFG is responsible for a suitable oxygen vacancy concentration, thus providing carrier for oxygen transport and decreasing the electron-transfer energy. Considering the different conditions of first-principles calculations (0 K) and actual operation (500-700 °C), the actual situation tends to more readily form oxygen vacancy than theoretical calculations. With this in mind, we sought to discuss the high oxygen vacancy concentration in the follow-up part of the study. The density of states (DOS) in oxygen-stoichiometric BSFG ($Ba_{0.75}Sr_{0.25}Fe_{0.875}Ga_{0.125}O_3$) and BSFG compositions was calculated to analyze the effect of oxygen vacancy. As shown in Figure 4c, as an indicator of adsorption-desorption ability of electrons, a larger integral size near Fermi level of BSFG over oxygen-stoichiometric BSFG is observed, which represents superior oxygen electrocatalytic activity. In addition, the O p-band center is a good descriptor for predicting experimental values of high-temperature surface exchange coefficient for perovskite materials. Herein, the calculated O p-band center for BSFG (δ in the range of [0.13, 0.17]) lies in the range of -1.48 to -1.59 eV, which exceeds that of LSCF and is comparable to that of BSCF (both are of potential commercial interest).[55] This indicates a high surface exchange coefficient, in turn correlating with improved ORR activity. Overall, the first-principles theoretical calculations further validate the activity and structural stability of BSFG perovskite oxide.

In conclusion, we have demonstrated A/B-site strontium and gallium co-substituted BSFG perovskite as an efficient cathode material with remarkable activity and durability for SOFCs. The well-defined cubic-symmetry structure, high oxygen vacancy content and rapid oxygen kinetics are in favor of the catalytic activity for ORR; while the well-preserved perovskite crystal lattice and acceptable thermal expansion behavior are expected to contribute to the operational stability. As a result, electrochemical evaluations of the cells constructed with BSFG exhibit a low polarization ASR of 0.074 Ω cm^2 and an exceptional PPD of 1145 mW cm^{-2} without noticeable performance degradation for 50 h at 600 °C. The electrochemical performance of BSFG cathode outperforms the widely available cobalt-free cathodes and even competes with the state-of-the-art cobalt-containing perovskites (such as BSCF). Additionally, the theoretical calculations further substantiate the activity and structural stability of BSFG for ORR. This work gives BSFG a significant advancement of oxygen reduction electrocatalysts for reduced-temperature SOFCs. Further work is ongoing to tailor the electrode/electrolyte architecture, determine cell operation under harsh conditions and assess long-term performance stability.

ASSOCIATED CONTENT

Supporting Information

The Supporting Information is available free of charge at .

Experimental details and additional characterization data (XRD, TEC, TGA, ECR, electrical conductivity, SEM, electrochemical test, and crystallographic details)

AUTHOR INFORMATION

Corresponding Authors

*E-mail: meng.ni@polyu.edu.hk.
*E-mail: zhanlin@gdut.edu.cn.

Author Contributions

The manuscript was written through contributions of all authors. All authors have given approval to the final version of the manuscript.

Notes

The authors declare no competing financial interest.

ACKNOWLEDGMENT

This work was financially supported by a startup R&D funding from One-Hundred Young Talents Program of Guangdong University of Technology, China (No.: 220413180), a Foundation for Youth Innovative Talents in Higher Education of Guangdong Province, China (No.: 2018KQNCX060), Joint Funds of Basic and Applied Basic Research Foundation of Guangdong Province, China (No. 2019A1515110322), grants from Research Grant Council, University Grants Committee, Hong Kong SAR (No. PolyU 152214/17E and PolyU 152064/18E).

REFERENCES

(1) Boldrin, P.; Brandon, N. P. Progress and outlook for solid oxide fuel cells for transportation applications. *Nat. Catal.* **2019**, *2*, 571-577.
(2) Duan, C.; Kee, R. J.; Zhu, H.; Karakaya, C.; Chen, Y.; Ricote, S.; Jarry, A.; Crumlin, E. J.; Hook, D.; Braun, R.; Sullivan, N. P.; O'Hayre, R. Highly durable, coking and sulfur tolerant, fuel-flexible protonic ceramic fuel cells. *Nature* **2018**, *557*, 217-222.
(3) Wachsman, E. D.; Lee, K. T. Lowering the temperature of solid oxide fuel cells. *Science* **2011**, *334*, 935-939.
(4) Chen, Y.; Choi, Y. M.; Yoo, S.; Ding, Y.; Yan, R.; Pei, K.; Qu, C.; Zhang, L.; Chang, I.; Zhao, B.; Zhang, Y.; Chen, H.; Chen, Y.; Yang, C.; deGlee, B.; Murphy, R.; Liu, J.; Liu, M. A highly efficient multiphase catalyst dramatically enhances the rate of oxygen reduction. *Joule* **2018**, *2*, 938-949.
(5) Li, M.; Zhao, M.; Li, F.; Zhou, W.; Peterson, V. K.; Xu, X.; Shao, Z.; Gentle, I.; Zhu, Z. A niobium and tantalum co-doped perovskite cathode for solid oxide fuel cells operating below 500 °C. *Nat. Commun.* **2017**, *8*, 13990.
(6) Chen, Y.; Zhou, W.; Ding, D.; Liu, M.; Ciucci, F.; Tade, M.; Shao, Z. Advances in cathode materials for solid oxide fuel cells: complex oxides without alkaline earth metal elements. *Adv. Energy Mater.* **2015**, *5*, 1500537.
(7) Yoo, S.; Jun, A.; Ju, Y.-W.; Odkhuu, D.; Hyodo, J.; Jeong, H. Y.; Park, N.; Shin, J.; Ishihara, T.; Kim, G. Development of double-perovskite compounds as cathode materials for low-temperature solid oxide fuel cells. *Angew. Chem. Int. Ed.* **2014**, *53*, 13064-13067.
(8) Jung, W.; Tuller, H. L. A new model describing solid oxide fuel cell cathode kinetics: model thin film $SrTi_{1-x}Fe_xO_{3-\delta}$ mixed conducting oxides-a case study. *Adv. Energy Mater.* **2011**, *1*, 1184-1191.

(9) Zhang, H.; Zhao, F.; Chen, F.; Xia, C. Nano-structured $Sm_{0.5}Sr_{0.5}CoO_{3-\delta}$ electrodes for intermediate-temperature SOFCs with zirconia electrolytes. *Solid State Ionics* **2011**, *192*, 591-594.
(10) Shao, Z.; Haile, S. M. A high-performance cathode for the next generation of solid-oxide fuel cells. *Nature* **2004**, *431*, 170-173.
(11) Wang, H.; Yakal-Kremski, K. J.; Yeh, T.; Rupp, G. M.; Limbeck, A.; Fleig, J.; Barnett, S. A. Mechanisms of performance degradation of $(La,Sr)(Co,Fe)O_{3-\delta}$ solid oxide fuel cell cathodes. *J. Electrochem. Soc.* **2016**, *163*, F581-F585.
(12) Ding, X.; Gao, Z.; Ding, D.; Zhao, X.; Hou, H.; Zhang, S.; Yuan, G. Cation deficiency enabled fast oxygen reduction reaction for a novel SOFC cathode with promoted CO_2 tolerance. *Appl. Catal. B: Environ.* **2019**, *243*, 546-555.
(13) Duan, C.; Hook, D.; Chen, Y.; Tong, J.; O'Hayre, R. Zr and Y co-doped perovskite as a stable, high performance cathode for solid oxide fuel cells operating below 500 °C. *Energy Environ. Sci.* **2017**, *10*, 176-182.
(14) Jun, A.; Kim, J.; Shin, J.; Kim, G. Achieving high efficiency and eliminating degradation in solid oxide electrochemical cells using high oxygen-capacity perovskite. *Angew. Chem. Int. Ed.* **2016**, *55*, 12512-12515.
(15) Boulahya, K.; Muñoz-Gil, D.; Gómez-Herrero, A.; Azcondoc, M. T.; Amador, U. $Eu_2SrCo_{1.5}Fe_{0.5}O_7$ a new promising Ruddlesden-Popper member as a cathode component for intermediate temperature solid oxide fuel cells. *J. Mater. Chem. A* **2019**, *7*, 5601-5611.
(16) Hashim, S. S.; Liang, F.; Zhou, W.; Sunarso, J. Cobalt-free perovskite cathodes for solid oxide fuel cells. *ChemElectroChem* **2019**, *6*, 3549-3569.
(17) Dong, F.; Chen, Y.; Chen, D.; Shao, Z. Surprisingly high activity for oxygen reduction reaction of selected oxides lacking long oxygen-ion diffusion paths at intermediate temperatures: a case study of cobalt-free $BaFeO_{3-\delta}$. *ACS Appl. Mater. Interfaces* **2014**, *6*, 11180-11189.
(18) Hombo, J.; Matsumoto, Y.; Kawano, T. Electrical conductivities of $SrFeO_{3-\delta}$ and $BaFeO_{3-\delta}$ perovskites. *J. Solid State Chem.* **1990**, *84*, 138-143.
(19) Hayashi, N.; Yamamoto, T.; Kageyama, H.; Nishi, M.; Watanabe, Y.; Kawakami, T.; Matsushita, Y.; Fujimori, A.; Takano, M. $BaFeO_3$: A ferromagnetic iron oxide. *Angew. Chem. Int. Ed.* **2011**, *50*, 12547-12550.
(20) Wang, J.; Saccoccio, M.; Chen, D.; Gao, Y.; Chen, C.; Ciucci, F. The effect of A-site and B-site substitution on $BaFeO_{3-\delta}$: An investigation as a cathode material for intermediate-temperature solid oxide fuel cells. *J. Power Sources* **2015**, *297*, 511-518.
(21) Baiyee, Z. M.; Chen, C.; Ciucci, F. A DFT+U study of A-site and B-site substitution in $BaFeO_{3-\delta}$. *Phys. Chem. Chem. Phys.* **2015**, *17*, 23511-23520.
(22) Dong, F.; Chen, D.; Chen, Y.; Zhao, Q.; Shao, Z. La-doped $BaFeO_{3-\delta}$ perovskite as a cobalt-free oxygen reduction electrode for solid oxide fuel cells with oxygen-ion conducting electrolyte. *J. Mater. Chem.* **2012**, *22*, 15071-15079.
(23) Dong, F.; Chen, Y.; Ran, R.; Chen, D.; Tadé, M. O.; Liu, S.; Shao, Z. $BaNb_{0.05}Fe_{0.95}O_{3-\delta}$ as a new oxygen reduction electrocatalyst for intermediate temperature solid oxide fuel cells. *J. Mater. Chem. A* **2013**, *1*, 9781-9791.
(24) Liu, H.; Zhu, K.; Liu, Y.; Li, W.; Cai, L.; Zhu, X.; Cheng, M.; Yang, W. Structure and electrochemical properties of cobalt-free perovskite cathode materials for intermediate-temperature solid oxide fuel cells. *Electrochim. Acta* **2018**, *279*, 224-230.
(25) Xia, W.; Li, Q.; Sun, L.; Huo, L.; Zhao, H. Enhanced electrochemical performance and CO_2 tolerance of $Ba_{0.95}La_{0.05}Fe_{0.85}Cu_{0.15}O_{3-\delta}$ as Fe-based cathode electrocatalyst for solid oxide fuel cells. *J. Eur. Ceram. Soc.* **2020**, *40*, 1967-1974.
(26) Lu, Y.; Zhao, H.; Li, K.; Du, X.; Ma, Y.; Chang, X.; Chen, N.; Zheng, K.; Świerczek, K. Effective calcium doping at the B-site of $BaFeO_{3-\delta}$ perovskite: towards low-cost and high-performance oxygen permeation membranes. *J. Mater. Chem. A* **2017**, *5*, 7999-8009.
(27) Jacobs, R.; Mayeshiba, T.; Booske, J.; Morgan, D. Material discovery and design principles for stable, high activity perovskite cathodes for solid oxide fuel cells. *Adv. Energy Mater.* **2018**, *8*, 1702708.
(28) Chen, K.; He, S.; Li, N.; Cheng, Y.; Ai, N.; Chen, M.; Rickard, W. D. A.; Zhang, T.; Jiang, S. P. Nb and Pd co-doped $La_{0.57}Sr_{0.38}Co_{0.19}Fe_{0.665}Nb_{0.095}Pd_{0.05}O_{3-\delta}$ as a stable, high performance electrode for barrier-layer-free Y_2O_3-ZrO_2 electrolyte of solid oxide fuel cells. *J. Power Sources* **2018**, *378*, 433-442.
(29) Gao, L.; Zhu, M.; Xia, T.; Li, Q.; Li, T.; Zhao, H. Ni-doped $BaFeO_{3-\delta}$ perovskite oxide as highly active cathode electrocatalyst for intermediate-temperature solid oxide fuel cells. *Electrochim. Acta* **2018**, *289*, 428-436.
(30) Ding, X.; Gao, X.; Zhu, W.; Wang, J.; Jiang, J. Electrode redox properties of $Ba_{1-x}La_xFeO_{3-\delta}$ as cobalt free cathode materials for intermediate-temperature SOFCs. *Int. J. Hydrogen Energy* **2014**, *39*, 12092-12100.
(31) Hong, T.; Zhao, M.; Brinkman, K.; Chen, F.; Xia, C. Enhanced oxygen reduction activity on Ruddlesden-Popper phase decorated $La_{0.8}Sr_{0.2}FeO_{3-\delta}$ 3D heterostructured cathode for solid oxide fuel cells. *ACS Appl. Mater. Interfaces* **2017**, *9*, 8659-8668.
(32) Pei, K.; Zhou, Y.; Xu, K.; He, Z.; Chen, Y.; Zhang, W.; Yoo, S.; Zhao, B.; Yuan, W.; Liu, M.; Chen, Y. Enhanced Cr-tolerance of an SOFC cathode by an efficient electro-catalyst coating. *Nano Energy* **2020**, *72*, 104704.
(33) Sun, C.; Kong, Y.; Shao, L.; Zhang, Q.; Wu, X.; Zhang, N.; Sun, K. Significant zirconium substitution effect on the oxygen reduction activity of the cathode material $NdBaCo_2O_{5+\delta}$ for solid oxide fuel cells. *ACS Sustainable Chem. Eng.* **2019**, *7*, 11603-11611.
(34) Li, L.; Yang, H.; Gao, Z.; Zhang, Y.; Dong, F.; Yang, G.; Ni, M.; Lin, Z. Nickel-substituted $Ba_{0.5}Sr_{0.5}Co_{0.8}Fe_{0.2}O_{3-\delta}$: a highly active perovskite oxygen electrode for reduced-temperature solid oxide fuel cells. *J. Mater. Chem. A* **2019**, *7*, 12343-12349.
(35) Lu, Y.; Zhao, H.; Chang, X.; Du, X.; Li, K.; Ma, Y.; Yi, S.; Du, Z.; Zheng, K.; Świerczek, K. Novel cobalt-free $BaFe_{1-x}Gd_xO_{3-\delta}$ perovskite membranes for oxygen separation. *J. Mater. Chem. A* **2016**, *4*, 10454-10466.
(36) Okiba, T.; Sato, T.; Fujishiro, F.; Niwa, E.; Hashimoto, T. Preparation of $Ba_{1-x}La_xFeO_{3-\delta}$ (x = 0.1-0.6) with cubic perovskite phase and random distribution of oxide ion vacancy and their electrical conduction property and thermal expansion behavior. *Solid State Ionics* **2018**, *320*, 76-83.
(37) Zhu, Y.; Zhou, W.; Chen, Y.; Shao, Z. An aurivillius oxide based cathode with excellent CO_2 tolerance for intermediate-temperature solid oxide fuel cells. *Angew. Chem. Int. Ed.* **2016**, *55*, 8988-8993.
(38) Zhang, Z.; Zhu, Y.; Zhong, Y.; Zhou, W.; Shao, Z. Anion doping: a new strategy for developing high-performance perovskite-type cathode materials of solid oxide fuel cells. *Adv. Energy Mater.* **2017**, *7*, 1700242.
(39) Gao, L.; Li, Q.; Sun, L.; Xia, T.; Huo, L.; Zhao, H.; Grenier, J.-C. Antimony-doped $Bi_{0.5}Sr_{0.5}FeO_{3-\delta}$ as a novel Fe-based oxygen reduction electrocatalyst for solid oxide fuel cells below 600 °C. *J. Mater. Chem. A* **2018**, *6*, 15221-15229.
(40) He, W.; Wu, X.; Dong, F.; Ni, M. A novel layered perovskite electrode for symmetrical solid oxide fuel cells: $PrBa(Fe_{0.8}Sc_{0.2})_2O_{5+\delta}$. *J. Power Sources* **2017**, *363*, 16-19.
(41) Liu, J.; Wang, J.; Belotti, A.; Ciucci, F. P-substituted $Ba_{0.95}La_{0.05}FeO_{3-\delta}$ as a cathode material for SOFCs. *ACS Appl. Energy Mater.* **2019**, *2*, 5472-5480.
(42) Hu, X.; Li, M.; Xie, Y.; Yang, Y.; Wu, X.; Xia, C. Oxygen-deficient Ruddlesden-Popper-type lanthanum strontium cuprate doped with bismuth as a cathode for solid oxide fuel cells. *ACS Appl. Mater. Interfaces* **2019**, *11*, 21593-21602.
(43) Lee, J. G.; Park, J. H.; Shul, Y. G. Tailoring gadolinium-doped ceria-based solid oxide fuel cells to achieve 2 W cm^{-2} at 550 °C. *Nat. Commun.* **2014**, *5*, 4045.
(44) Chen, Y.; Yoo, S.; Choi, Y. M.; Kim, J. H.; Ding, Y.; Pei, K.; Murphy, R.; Zhang, Y.; Zhao, B.; Zhang, W.; Chen, H.; Chen, Y.; Yuan, W.; Yang, C.; Liu, M. A highly active, CO_2-tolerant electrode for the oxygen reduction reaction. *Energy Environ. Sci.* **2018**, *11*, 2458-2466.
(45) Li, M.; Niu, H.; Druce, J.; Téllez, H.; Ishihara, T.; Kilner, J. A.; Gasparyan, H.; Pitcher, M. J.; Xu, W.; Shin, J. F.; Daniels, L. M.; Jones, L. A. H.; Dhanak, V. R.; Hu, D.; Zanella, M.; Claridge, J. B.; Rosseinsky, M. J. A CO_2-tolerant perovskite oxide with high oxide ion and electronic conductivity. *Adv. Mater.* **2020**, *32*, 1905200.

(46) Chen, Y.; Bu, Y.; Zhang, Y.; Yan, R.; Ding, D.; Zhao, B.; Yoo, S.; Dang, D.; Hu, R.; Yang, C.; Liu, M. A highly efficient and robust nanofiber cathode for solid oxide fuel cells. *Adv. Energy Mater.* **2017**, *7*, 1601890.
(47) Rehman, A.U.; Li, M.; Knibbe, R.; Khan, M. S.; Peterson, V. K.; Brand, H. E. A.; Li, Z.; Zhou, W.; Zhu, Z. Enhancing oxygen reduction reaction activity and CO_2 tolerance of cathode for low-temperature solid oxide fuel cells by in situ formation of carbonates. *ACS Appl. Mater. Interfaces* **2019**, *11*, 26909-26919.
(48) Dong, F.; Ni, M.; He, W.; Chen, Y.; Yang, G.; Chen, D.; Shao, Z. An efficient electrocatalyst as cathode material for solid oxide fuel cells: $BaFe_{0.95}Sn_{0.05}O_{3-\delta}$. *J. Power Sources* **2016**, *326*, 459-465.
(49) Huan, D.; Wang, Z.; Wang, Z.; Peng, R.; Xia, C.; Lu, Y. High-performanced cathode with a two-layered R-P structure for intermediate temperature solid oxide fuel cells. *ACS Appl. Mater. Interfaces* **2016**, *8*, 4592-4599.
(50) Zhang, S.-L.; Wang, H.; Lu, M. Y.; Zhang, A.-P.; Mogni, L. V.; Liu, Q.; Li, C.-X.; Li, C.-J.; Barnett, S. A. Cobalt-substituted $SrTi_{0.3}Fe_{0.7}O_{3-\delta}$: a stable high-performance oxygen electrode material for intermediate-temperature solid oxide electrochemical cells. *Energy Environ. Sci.* **2018**, *11*, 1870-1879.
(51) Song, Y.; Chen, Y.; Xu, M.; Wang, W.; Zhang, Y.; Yang, G.; Ran, R.; Zhou, W.; Shao, Z. A cobalt-free multi-phase nanocomposite as near-ideal cathode of intermediate-temperature solid oxide fuel cells developed by smart self-assembly. *Adv. Mater.* **2020**, *32*, 1906979.
(52) He, W.; Wu, X.; Yang, G.; Shi, H.; Dong, F.; Ni, M. $BaCo_{0.7}Fe_{0.22}Y_{0.08}O_{3-\delta}$ as an active oxygen reduction electrocatalyst for low-temperature solid oxide fuel cells below 600 °C. *ACS Energy Lett.* **2017**, *2*, 301-305.
(53) Zhou, Y.; Wu, H.; Luo, T.; Wang, J.; Shi, Y.; Xia, C.; Wang, S.; Zhan, Z. A nanostructured architecture for reduced-temperature solid oxide fuel cells. *Adv. Energy Mater.* **2015**, *5*, 1500375.
(54) Kang, B. S.; Matsuda, J.; Ju, Y. W.; Kim, H. H.; Ishihara, T. Nano strain induced double columnar oxide as highly active oxygen-dissociation electrode for Ni-Fe metal supported solid oxide fuel cells. *Nano Energy* **2019**, *56*, 382-390.
(55) Lee, Y.-L.; Kleis, J.; Rossmeisl, J.; Shao-Horn, Y.; Morgan, D. Prediction of solid oxide fuel cell cathode activity with first-principles descriptors. *Energy Environ. Sci.* **2011**, *4*, 3966-3970.

Table of Contents artwork